Table 2. Proportion of DNA complementary to the rRNA in 70*S* and 80*S* ribosomes for four *Nicotiana* species and the calculated number of cistrons per cell for each type of rRNA. The values for the proportion of DNA complementary to the rRNA in 80*S* ribosomes were obtained by hybridizing an excess of tobacco root rRNA to nuclear DNA's of the four species. This is possible because roots contain only 80*S* ribosomes (*15, 19*). Values for 70*S* rDNA's were obtained by subtracting the proportion of 80*S* rDNA from that listed in Table 1 for total proportion of rDNA (*7, 15*). The subtraction method was used for convenience and because it yields the same value for tobacco 70*S* rDNA as does the more direct determination using radioactive RNA from purified 70*S* ribosomes (*20*); CN, chromosome number.

Species	CN	DNA per nucleus (pg)	Percentage of DNA complementary to		Number of cistrons for	
			80*S* rRNA	70*S* rRNA	80*S* rRNA	70*S* rRNA
N. tabacum	48	10.1	0.15	0.13	4,500	4,600
N. occidentalis	42	9.4	0.13	0.30	3,700	10,000
N. paniculata	24	4.5	0.26	0.54	3,500	8,600
N. sylvestris	24	5.1	0.27	0.63	4,100	11,300

dense, rDNA-containing satellite component when subjected to isopycnic centrifugation in cesium chloride, whereas the DNA of *N. tabacum*, with a relatively low genomic proportion of rDNA, lacks such a visible satellite component (*4, 7*). The DNA's of the ten *Nicotiana* species examined here were subjected to analytical isopycnic centrifugation; as might have been predicted, the diploid species all displayed a clearly definable satellite component whereas none was visible for the tetraploids.

Perhaps there is a physiological requirement for a constant number of rRNA cistrons per cell, so that the different genomic proportions of rDNA may be a consequence of a constant number of cistrons but different amounts of DNA per cell. Cell DNA content was determined for diploid and tetraploid species in order to test this hypothesis. Leaf blade cells were separated with pectinase (*8*), counted with the aid of a hemocytometer, and treated to remove color and lipids (*9*); and DNA was measured (*10*). It was found, in agreement with others (*11*), that the tetraploid species *N. tabacum* contains 10.1 pg of DNA per cell and that the value for another tetraploid species, *N. occidentalis*, is 9.4 pg per cell. On the other hand, diploid species *N. sylvestris* and *N. paniculata* contain, respectively, 5.1 and 4.5 pg per cell. It is to be expected that a doubling of chromosome number leads to a doubling of cell DNA content, but the fact that the proportion of rDNA is lower in tetraploids than in diploids indicates that either rDNA does not double wth the rest of the genome during tetraploidization or that some of it is preferentially lost after the doubling event. The latter possibility seems more likely because the tetraploid species have arisen as amphidiploids (*6*).

There are two types of ribosomes in plants, chloroplastic 70*S* and cytoplasmic 80*S* ribosomes (*12*). The 70*S* ribosomes contain 23*S* and 16*S* RNA species of high molecular weight, whereas the 80*S* ribosomes contain 25*S* and 18*S* RNA species (*13*). The proportions of the genomes complementary to the RNA's of the two types of ribosomes are listed in Table 2 for four *Nicotiana* species; cell DNA content was determined along with the calculated number of cistrons per nucleus. The numbers of cistrons for the cytoplasmic rRNA's are similar for the four species, even though they have different chromosome numbers and DNA contents. However, wide variation is seen in the numbers of cistrons for the 70*S* rRNA's, the highest and lowest values differing by a factor of 2.5. The data suggest that there is a constancy in number of cistrons for cytoplasmic rRNA's in closely related plant species, even though these species may differ in chromosome number and cell DNA content; whereas the number of cistrons for the chloroplast ribosomes varies considerably.

These data, which indicate little variation in number of cistrons for 80*S* rRNA even when the genomic proportion of rDNA varies, apply to species belonging to a single genus, *Nicotiana*. However, two survey studies, one with plants (*3*) and the other with animals (*2*), demonstrate that even when species in disparate genera are compared, the genomic proportion of rDNA varies considerably more than does the actual number of rRNA cistrons.

ALBERT SIEGEL*, DONALD LIGHTFOOT†
Department of Agricultural Biochemistry, University of Arizona, Tucson 85721
OSCAR G. WARD, SHERRY KEENER
Genetics Program, University of Arizona

References and Notes

1. M. Birnstiel, M. Chipchase, J. Spiers, *Progr. Nucleic Acid Res. Mol. Biol.* **11**, 351 (1971); J. Sinclair and D. Brown, *Biochemistry* **10**, 2761 (1971).
2. R. Pederson, *J. Exp. Zool.* **177**, 65 (1971).
3. J. Ingle and J. Sinclair, *Nature* **235**, 30 (1972).
4. K. Matsuda and A. Siegel, *Proc. Nat. Acad. Sci. U.S.A.* **58**, 673 (1967).
5. R. Goldberg and A. Siegel, *Genetics* **72**, 253 (1972).
6. T. Goodspeed, *The Genus Nicotiana* (Chronica Botanica, Waltham, Mass., 1954).
7. K. Matsuda, A. Siegel, D. Lightfoot, *Plant Physiol.* **46**, 6 (1970).
8. R. Jensen, R. Francki, M. Zaitlin, *ibid.* **48**, 9 (1971).
9. R. Smillie and G. Krotkov, *Can. J. Bot.* **38**, 31 (1960).
10. K. Burton, *Biochem. J.* **62**, 315 (1956).
11. W. Flamm and M. Birnstiel, *Biochim. Biophys. Acta* **87**, 101 (1964).
12. J. Lyttleton, *Exp. Cell Res.* **26**, 312 (1962).
13. U. Loening and J. Ingle, *Nature* **215**, 363 (1967).
14. D. Gillespie and S. Spiegelman, *J. Mol. Biol.* **12**, 829 (1965).
15. D. Lightfoot, thesis, University of Arizona (1972).
16. W. Flamm, H. Bond, H. Burr, *Biochim. Biophys. Acta* **129**, 310 (1966).
17. M. Zaitlin, D. Spencer, P. Whitfield, in *Proceedings of the International Symposium on Plant Biochemical Regulation in Viral and Other Disease or Injury* (Phytopathology Society of Japan, Tokyo, 1968), pp. 91–103.
18. D. Baltimore, *J. Mol. Biol.* **18**, 421 (1966).
19. T. C. Hsiao, *Biochim. Biophys. Acta* **91**, 598 (1964).
20. K. Tewari and S. G. Wildman, *Symp. Soc. Exp. Biol.* **24**, 147 (1970).
21. Supported by an NSF grant and by AEC contract (11-1)-873. This is Paper No. 1957 from the Arizona Agricultural Experiment Station.
* Present address: Biology Department, Wayne State University, Detroit, Mich. 48202.
† Present address: Department of Biochemistry, University of California, Riverside 92502.

5 July 1972; revised 20 November 1972

Aqueous Central Cavity in Aspartate Transcarbamylase from Escherichia coli

Abstract. *A three-dimensional x-ray diffraction study of aspartate transcarbamylase to 5.5-angstrom resolution, with the aid of four isomorphous heavy atom derivatives, indicates the presence of a central aqueous cavity approximating an oblate spheroid about 25 by 50 by 50 angstroms in dimension, within a molecule about 90 by 110 by 110 angstroms in largest dimensions.*

Aspartate transcarbamylase catalyzes the formation of carbamyl aspartate from carbamyl phosphate and aspartate (*1*). Cytidine triphosphate (CTP), a later product along the pathway for pyrimidine biosynthesis, inhibits this enzyme obtained from *Escherichia coli* (*2, 3*). Also, adenosine triphosphate, a

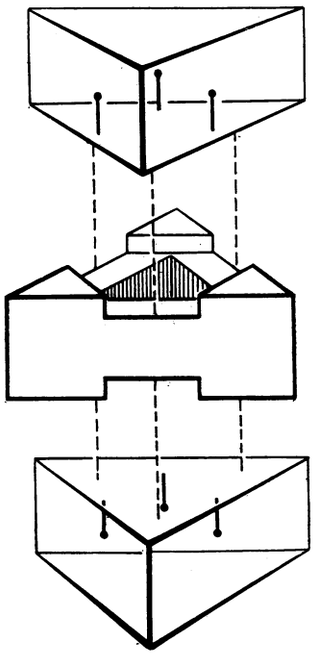

Fig. 1. Expanded view of the aspartate transcarbamylase molecule, showing a schematic representation of the major part of the catalytic trimers C_3 above and below, and the mostly regulatory region between. The assembled molecule has a central cavity (shaded region) about 25 Å along the threefold direction (3) and about 50 Å along the twofold direction (2). The molecular center is halfway along these dimensions. The overall molecular dimensions are about 90 Å along 3 and 110 Å along the 2's. The largest openings from the outside to the central cavity are the six 15-Å channels in the regulatory region. Some of the central region near the ends of the dashed lines may be part of the C_3 units, which may be nearly in contact with each other. Dots within the C_3 units represent the Hg sites, which are easily accessible from the central cavity. This diagram is not meant to imply the sequential order of assembly of the two C_3 and three R_2 units of the molecule.

purine, stimulates aspartate transcarbamylase, competing with CTP for the regulatory site (*3*, *4*). The regulatory (R) sites and catalytic (C) sites are on different proteins (*5*) in this allosteric enzyme.

The hexameric nature R_6C_6 of this aspartate transcarbamylase (molecular weight, 310,000) was established by a combination of x-ray diffraction results (*6*), with molecular weights of C and R along with sequence analysis (*7*) of the regulatory subunit. The molecular symmetry is D_3 (*8*). Spatial distribution of the catalytic trimers relative to the regulatory regions as established by the x-ray study (*8*) has recently been confirmed by electron microscopy (*9*). We have now obtained a greatly improved electron density map at 5.5 Å resolution which reveals the existence of a large central aqueous cavity in the aspartate transcarbamylase molecule (*8*).

Heavy atom parameters for the four derivatives of aspartate transcarbamylase given in Table 1, where fractional coordinates refer to the unit cell dimensions $a = 131$ Å and $c = 200$ Å in the space group, $R32$. A brief summary of the statistics of phasing (Table 2) indicates that the figure of merit (0.77) is considerably improved over that (0.59) of our earlier results (*8*) obtained only with the Hg and Au derivatives. The electron density map is greatly improved, showing erroneous features less than 6 Å in size at the contour level of 0.14 e Å^{-3}, where the highest density features are about 0.5 e Å^{-3} (F_{000} not included).

This map confirms the molecular boundaries (*8*) and the earlier tentative locations of the catalytic trimers and

Table 1. Heavy atom parameters. The absolute hand of the entire heavy atom constellation, and thus of the protein map, has not yet been determined.

Site No.	Occupancy (%)	Fractional coordinates		
		x	y	z
2-Chloromercuri-4-nitrophenol (8)				
1	95	0.089	0.100	0.104
$KAu(CN)_2$, 6.2×10^{-3}M*				
1	64	.082	.133	.097
2	20	.275	.126	.028
3	10	.121	.201	.052
4	13	.728	.251	.155
5	11	.056	.267	.009
$IrBr_6$, 10^{-2}M*				
1	79	.008	.153	.071
2	38	.040	.130	.074
3	27	.272	.069	.093
4	18	.124	.069	.125
5	9	.333	.091	.100
K_2PtCl_4, 10^{-3}M†				
1	96	.329	.078	.102
2	37	.0	.0	.157
3	55	.840	.468	.010
4	31	.333	.006	.112
5	24	.053	.105	.075
6	16	.905	.294	.163
7	15	.024	.312	.015

* Buffer, 0.05*M* imidazole and 0.05*M* tris·HCl, *p*H 6.35. † Buffer, 0.1*M* triethanolamine·HCl, *p*H 6.35.

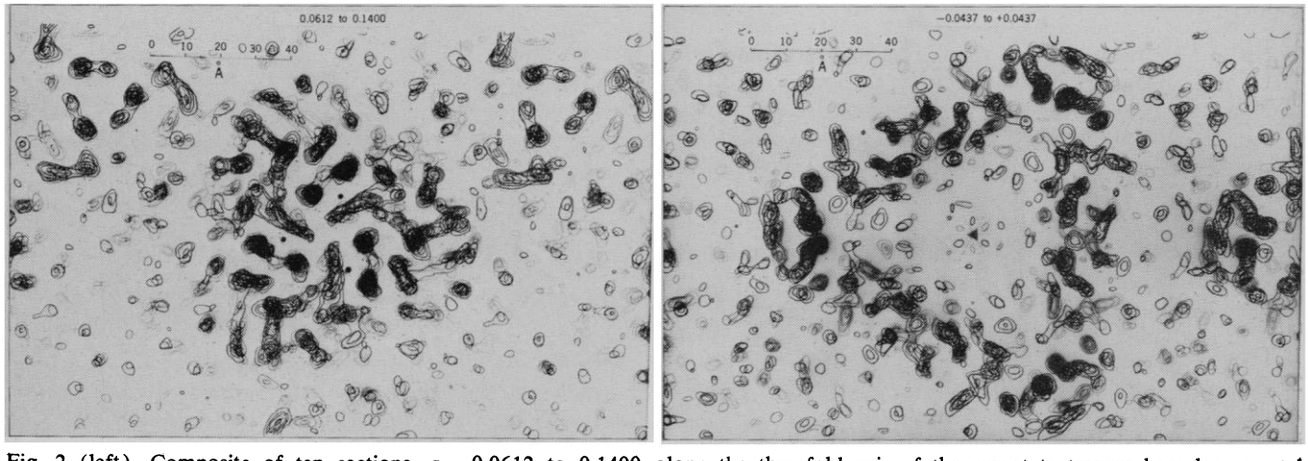

Fig. 2 (left). Composite of ten sections, $a = 0.0612$ to 0.1400 along the threefold axis of the aspartate transcarbamylase crystal and in the region of the triangular catalytic trimer. The three Hg sites are within a C_3 unit and are indicated by small black dots. Helical regions along the threefold direction appear as dense features about 6 Å in size, while elongated connected features are helices inclined with respect to the threefold axis. The density in the upper corners of this figure is associated with adjacent molecules. Fig. 3 (right). Composite of 11 sections, $z = -0.0437$ to 0.0437 along the threefold axis of aspartate transcarbamylase. The molecular center is in section zero, at the center of the internal cavity of the molecule. Regions of electron density furthest from the molecular center are interpreted as a major part of the regulatory units, but it is possible that some of the density shown here is associated with the catalytic protein. The density to the extreme right is part of a different molecule in the crystal.

Table 2. Statistics of phasing. The figure of merit (mean value of the cosine of the phase angle error) is $\overline{M} = 0.77$ for this refinement, in which scale factors were refined for each reciprocal lattice level (that is, photograph) for the protein and derivative.

Derivative	RMS F_c,* electrons	RMS E,† electrons
Hg	476	216
Au	351	219
Pt	688	336
Ir	451	299

* Root mean square (RMS) $F_c = [\Sigma_j h^2/n]^{1/2}$, where f_{hj} is the heavy-atom scattering amplitude for reflection h of derivative j; n is the total number of reflections. The RMS structure factor of the native protein is 2870 electrons. † RMS $E = [\Sigma \epsilon_{hj}^2/n]^{1/2}$, where ϵ_{hj} is the lack of closure for reflection h of derivative j.

the regulatory region (Figs. 1 to 3). We see no conflict between our earlier maps (*8*) (or our present maps) and the electron micrographs obtained by Richards and Williams (*9*). We do not, however, fully agree with the interpretation (*10*) by Cohlberg *et al.* in which the R chains are represented by long rod-shaped "arms" 20 by 60 Å. We find that the regulatory dimer is more nearly globular in shape. The highly stained region within the molecule [figure 1 in (*9*)] which creates the appearance of "arms" can, in view of the x-ray results, be accounted for by (i) the accumulation of the stain in the central cavity and (ii) the relative thinness of stain-excluding protein in the R:C interface (see Fig. 4). Similarly, micrographs of the molecule viewed perpendicular to the threefold axis show a central dark staining region [figure 2 in (*9*)], which can now be interpreted as the central cavity.

One striking feature of the new map is the helix content, estimated as about 35 percent for the C unit and 10 percent for the R unit. Uncertainties in these numbers arise partly from the ambiguities in assigning the electron density in the region of contact between these units, and from lack of resolution of small helical regions.

A schematic drawing of the assembly of the two C_3 units and the regulatory units around the central cavity of aspartate transcarbamylase is shown in Fig. 1. This cavity has dimensions of about 25 Å along the threefold and about 50 Å along the three twofold axes (including both directions from the molecular center). A revision of the earlier interpretation is that the possible channel (*8*) along the threefold axis is now completely filled with protein density. The largest remaining channels to the central cavity are six openings, each 15 Å in diameter. These openings are

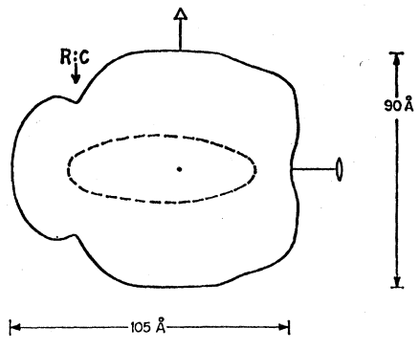

Fig. 4. Side view of the aspartate transcarbamylase molecule perpendicular to the threefold and one twofold axes, showing the central cavity and one regulatory dimer (left side). The boundary between regulatory and catalytic regions is suggested by the symbol R:C.

located near the median plane of the molecule in the region containing predominately R chains but also portions of the C chain.

Reaction of aspartate transcarbamylase with 2-chloromercuri-4-nitrophenol results in loss of enzyme activity, and does not dissociate the aspartate transcarbamylase molecule (*11*). It is likely that the thiol group which reacts with this mercurial is near the active site inasmuch as this derivative no longer binds succinate (*12*), although this thiol is not directly involved in binding or catalysis (*13*). According to the density map, this Hg site is easily accessible from the central cavity, but probably not directly from the outside of the aspartate transcarbamylase molecule.

A number of conformational changes are implicated in the catalytic and regulatory activities of aspartate transcarbamylase. An appealing possibility, suggested by our x-ray structure study, is that access to the central cavity of this enzyme is regulated by its interaction with CTP (and with adenosine triphosphate) (*14*). Central cavities in enzyme complexes may simply arise as a consequence of packing protein subunits around positions of high symmetry, like the 32 position in aspartate transcarbamylase. Further studies of this enzyme and of its complexes with effectors are under way in order to elucidate these mechanisms at the level of atomic resolution.

D. R. Evans, S. G. Warren
B. F. P. Edwards, C. H. McMurray
P. H. Bethge, D. C. Wiley
W. N. Lipscomb

Department of Chemistry,
Harvard University,
Cambridge, Massachusetts 02138

References and Notes

1. M. E. Jones, L. Spector, F. Lipmann, *J. Amer. Chem. Soc.* **77**, 819 (1955); P. Reichard and G. Hanshoff, *Acta Chem. Scand.* **10**, 548 (1956).
2. R. A. Yates and A. B. Pardee, *J. Biol. Chem.* **221**, 757 (1956).
3. J. C. Gerhart and A. B. Pardee, *ibid.* **237**, 891 (1962).
4. ———, *Fed. Proc.* **23**, 727 (1964).
5. J. C. Gerhart and H. K. Schachman, *Biochemistry* **4**, 1054 (1965).
6. D. C. Wiley and W. N. Lipscomb, *Nature* **218**, 1119 (1968).
7. K. Weber, *ibid.*, p. 1118.
8. D. C. Wiley, D. R. Evans, S. G. Warren, C. H. McMurray, B. F. P. Edwards, W. A. Franks, W. N. Lipscomb, *Cold Spring Harbor Symp. Quant. Biol.* **36**, 285 (1971).
9. K. E. Richards and R. C. Williams, *Biochemistry* **11**, 3393 (1972).
10. J. A. Cohlberg, V. P. Pigiet, Jr., H. K. Schachman, *ibid.*, p. 3396.
11. D. R. Evans, C. H. McMurray, W. N. Lipscomb, *Proc. Nat. Acad. Sci. U.S.A.* **69**, 3638 (1972).
12. C. H. McMurray, D. R. Evans, B. D. Sykes, *Biochem. Biophys. Res. Commun.* **48**, 572 (1972).
13. T. C. Vanaman and G. R. Stark, *J. Biol. Chem.* **245**, 3565 (1970).
14. The relative positions of the zinc ions and the C-chain SH-groups have been determined in crystals (*6*) of the CTP-aspartate transcarbamylase complex. Each zinc ion is 24 Å away from the nearest C-chain SH-group.
15. We thank the National Institutes of Health and the Guggenheim Foundation for support of this research. A preliminary account of this research was given at the third Enzyme Conference, at the University of California, Los Angeles, 27 to 29 December 1972.

15 January 1973

Sea Urchin Sperm-Egg Interactions Studied with the Scanning Electron Microscope

Abstract. *Scanning electron microscopy of the outer surface of sea urchin eggs sampled at intervals during the first 3 minutes after insemination reveals the detailed structural changes of the vitelline layer during its transformation into the fertilization membrane. A sperm attachment-detachment sequence is described for the large number of sperm which transitorily bind every egg during fertilization.*

After insemination of the eggs of the purple sea urchin, *Strongylocentrotus purpuratus*, there is a 25-second latent period before the first morphological response of the egg in fertilization is initiated (*1, 2*). This response is cortical granule breakdown, which begins at the site of successful sperm penetration and propagates around the egg in the next 20 to 30 seconds (*3*). During the latent